Laminar flame propagation modeling using the Radial Basis Function (RBF) method

V. Bayona & M. Kindelan
Universidad Carlos III de Madrid, Spain

Abstract

In this work we explore the applicability of the RBF method to laminar flame propagation modeling. This method is specially well suited for the solution of problems with complex geometries and irregular boundaries where spectral methods can not be applied. Another important advantage is that the method is independent of the dimension of the problem and, therefore, it is very easy to apply in 3D problems with complex geometries. We use both the global and the local (RBF-FD) versions of the method and we show its applicability in the solution of flame propagation problems in one, two and three dimensions using equispaced and non-equispaced nodes.
Keywords: flame propagation, Meshless methods, RBF global method, RBF-FD.

1 Introduction

Premixed flame propagation is an important topic in combustion research with many applications in engineering and industry safety. Thus, it is important to understand this physical process which very often takes place in complex shaped domains. One important tool to achieve this goal is the numerical simulation of the equations describing flame propagation. The purpose of this work is to explore the applicability of RBF methods to laminar flame propagation modeling. The main feature of these methods is its mesh-independence, relying not on the location but on the distance between RBF centers. This fact makes RBF methods basically the same for any dimension and for any shape of the domain. Furthermore, they are conceptually simple and easy to implement. There are two different formulations of the RBF method: the global RBF method [1, 2] and the local RBF method [3–5] also known as RBF-generated finite differences (RBF-FD).

In the global RBF formulation, full differentiation matrices are constructed based on RBF interpolants. This formulation is spectrally convergent independently of the distribution of RBF centers. Its principal drawback is that, as the overall number of centers increases, the condition number of the differentiation matrix increases, and this fact restricts the applicability of the method to large scale problems where a great number of RBF centers. In the RBF-FD formulation, the spectral convergence is lost. However, the method has the great advantage that the resulting differentiation matrices are sparse and well-conditioned even for large scale problems in complexly shaped domains. Accuracy is strongly dependent on the shape parameter of the RBF. References [6] and [7] address the problem of optimal selection of the shape parameter in the global RBF and RBF-FD method respectively.

2 Thermo-diffusive model of flame propagation

The thermo-diffusive model of flame propagation in ducts can be written as

$$\frac{\partial T}{\partial t} = \Delta T + \omega(T, Y) \tag{1}$$

$$\frac{\partial Y}{\partial t} = \frac{1}{\mathrm{Le}} \Delta Y - \omega(T, Y) \tag{2}$$

where Δ is the laplacian, Y the mass fraction of the reactant, T the non-dimensional temperature, and $\omega(T, Y)$ the nondimensional reaction rate which is assumed to follow an Arrhenius law of the form

$$\omega(T, Y) = \frac{\beta^2}{2 \, \mathrm{Le} \, u_p^2} Y \, \exp\left(\frac{\beta \, (T - 1)}{1 + \alpha(T - 1)}\right) \tag{3}$$

The non-dimensional parameters Le, β, u_p and α are the Lewis number, the Zeldovich number, the planar flame burning velocity and the heat release ratio, respectively. In reference [8] the following asymptotic formula for the planar burning velocity was derived,

$$u_p = 1 - \frac{3 \, \alpha - 2.344 + \mathrm{Le}}{\beta} + O(\beta^{-2})$$

In the rest of the paper we will consider $\beta \gg 1$ and, therefore, we will assume $u_p = 1$. Alternatively, these equations can be written in a moving frame [9] by adding the corresponding convective terms, $V(t) \dfrac{\partial T}{\partial z}$, $V(t) \dfrac{\partial Y}{\partial z}$, where z is the coordinate along the duct, and $V(t)$ is the velocity of the moving frame, usually chosen as the flame propagation velocity. In this way, the flame appears as stationary in the moving frame.

In the following, we present some numerical experiments to check the results of the analyses of the instability of the propagation of a plane flame front carried out by Sivashinsky [10, 11]. The main result being that if the inequality $\mathrm{Le} \leq 1 - 2/\beta$

holds, then the flame is unstable to perturbations whose wavelength is larger than $\lambda_0 = \eta \, \pi \, / \, \sqrt{\eta - 1}$, where $\eta = (\beta/2)\,(1 - \text{Le})$. Thus, in two dimensions, we will use the following initial and boundary conditions

$$T(y, z, 0) = \begin{cases} \exp\,(z - f(y)) & \text{if } z \leq f(y) \\ 1 & \text{if } z > f(y) \end{cases}, \tag{4}$$

$$Y(y, z, 0) = \begin{cases} 1 - \exp\,[\text{Le}(z - f(y))] & \text{if } z \leq f(y) \\ 0 & \text{if } z > f(y) \end{cases}, \tag{5}$$

$$T(y, -\infty, t) = 1 - Y(y, -\infty, t) = 0\,, \tag{6}$$

$$T(y, \infty, t) = 1 - Y(y, \infty, t) = 1\,, \tag{7}$$

$$\frac{\partial T}{\partial y}(\pm R, z, t) = \frac{\partial Y}{\partial y}(\pm R, z, t) = 0 \tag{8}$$

where y and z are the transversal and longitudinal coordinates respectively, R is the duct width, $f(y) = \mu \, \cos\,(2\,\pi\,y\,/\,\lambda)$, and λ is the wavelength of the perturbation to the flame front. Changing λ changes the wavelength of the perturbation. If $\lambda = \infty$, the initial profile is a flat temperature and mass fraction front.

2.1 RBF global method

To solve equations (1-2), we look for an approximate solution in the space spanned by a set of translated Radial Basis Functions (RBF). Thus,

$$T(t,\,\mathbf{x}) = \sum_{k=1}^{N} a_k(t)\,\phi_k(r_k(\mathbf{x}), c_T) \tag{9}$$

$$Y(t,\,\mathbf{x}) = \sum_{k=1}^{N} b_k(t)\,\phi_k(r_k(\mathbf{x}), c_Y) \tag{10}$$

where $\mathbf{x}$ represents the vector (y, z), $\{\mathbf{x}_k\}$, $k = 1, \dots, N$ is a set of N RBF centers, $r_k(\mathbf{x}) = \| \, \mathbf{x} - \mathbf{x}_k \, \|$ is the distance to the RBF center, and $\phi_k(r_k(\mathbf{x}), c)$ is an RBF function centered at $\mathbf{x_k}$. As RBFs, we use Hardy's multiquadrics [12]

$$\phi_k(\| \, \mathbf{x} - \mathbf{x}_k \, \|, c) = \sqrt{(y - y_k)^2 + (z - z_k)^2 + c^2}\,. \tag{11}$$

The coefficients $a_k(t)$ and $b_k(t)$ are computed by collocation of (9-10) into the PDE (1-2) and into the boundary conditions (6-8). At interior nodes, equation (1) leads to

$$\sum_{k=1}^{N} a'_k(t)\,\phi_k(r_k(\mathbf{x}_i), c_T) = \sum_{k=1}^{N} a_k(t)\,\Delta\phi_k(r_k(\mathbf{x}_i), c_T) + \omega(T, Y)\,. \tag{12}$$

At boundary nodes corresponding to $z = \pm\infty$, equations (6-7) lead to

$$\sum_{k=1}^{N} a'_k(t)\, \phi_k(r_k(\mathbf{x}_i), c_T) = 0. \tag{13}$$

Similar equations are obtained for the mass fraction Y by using $b'_k(t)$ and $b_k(t)$ instead of $a'_k(t)$ and $a_k(t)$.

The boundary condition (8) implies

$$0 = \sum_{k=1}^{N} a_k(t)\, \frac{\partial \phi_k(r_k(\mathbf{x}_i), c_T)}{\partial y}. \tag{14}$$

These equations can be written in matrix form as

$$M \begin{bmatrix} \mathbf{a} \\ \mathbf{b} \end{bmatrix}' = \mathbf{f}(\mathbf{a}, \mathbf{b}) \tag{15}$$

where the mass matrix M has dimensions $(2N) \times (2N)$. The elements M_{ik} in rows of M corresponding to interior nodes (12) or to boundary nodes at $z = \pm\infty$ (13) have values $\phi_k(r_k(\mathbf{x}_i), c)$. The elements M_{ik} in rows of M corresponding to lateral boundary nodes (14) are zero. Thus, matrix M is singular and therefore equation (15) is a differential-algebraic equation (DAE). To solve it we use Matlab's function `ode23t` which can solve DAEs of index 1.

The right-hand side vector $\mathbf{f}$ at interior nodes has the value,

$$f_i(\mathbf{a}, \mathbf{b}) = \sum_{k=1}^{N} a_k(t)\, \Delta\phi_k(r_k(\mathbf{x}_i), c_T) + \omega(T, Y) \tag{16}$$

for rows corresponding to temperature ($i \leq N$). For rows corresponding to mass fraction at interior nodes ($i > N$) there is an analogous expression with b_i replacing a_i and with the Lewis number Le dividing the first term in the right-hand side, and with a minus sign in front of the reaction term ω. For boundary nodes, f_i has the value 0 or 1 depending on the boundary condition.

To start the time integration of equation (15) appropriate initial values for $\mathbf{a}_0$ and $\mathbf{b}_0$ are needed. These are obtained by RBF interpolation of the initial distribution of temperature (4) and mass fraction (5) complying with boundary condition (8).

2.1.1 Numerical results
The initial profiles for temperature and mass fraction (4, 5) exhibit a discontinuity in the first derivative at the location of the flame front. RBF interpolation of these initial profiles to compute the initial values of $\mathbf{a}_0$ and $\mathbf{b}_0$, results in initial distributions of temperature and mass fraction with large oscillatory behavior near the discontinuity. This is due to a Runge type phenomenon, which is well known to occur in RBF interpolation [13, 14]. This is not surprising since in the limit of
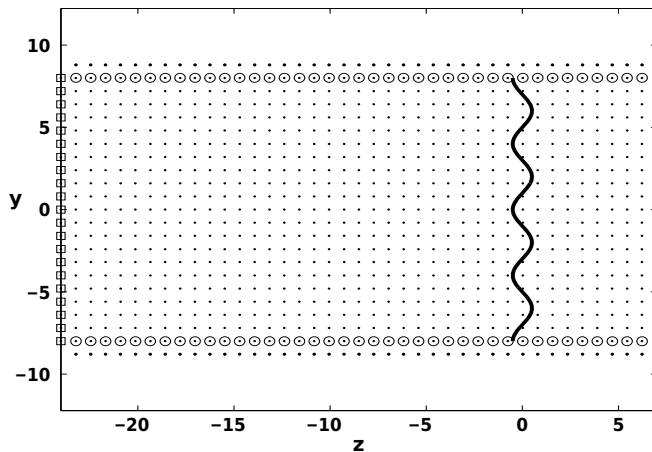
Figure 1: RBF nodes (·) and collocation nodes: (□) equation (13), (○) equation (14).

large shape parameter, RBF interpolation is equivalent to Lagrange polynomial interpolation where the Runge phenomenon is well known.

One alternative to eliminate the Runge phenomenon is to use the method that was proposed by Fedoseyev *et al.* [15]. It is based on enforcing collocation of the PDE in boundary nodes, so that both the boundary condition and the PDE are imposed in those nodes. In our case we use Fedoseyev's method only in lateral boundary nodes. However, since the number of equations increases, it is necessary to introduce additional RBF centers to match the number of unknown coefficients. Figure 1 shows the nodes that we have used to implement the method. There are $n_z = 41$, $n_y = 21$ equispaced nodes in the longitudinal and transversal direction. There are also 78 additional RBF centers which are located outside the domain at distance Δy from the corresponding boundary nodes. Thus, in this case we use $861 + 78 = 939$ RBF centers. Equation (15) is a 1878×1878 system of differential-algebraic equations of index 1. Also shown in Figure 1 is the initial flame location $f(y) = \mu \cos(2\pi y / \lambda)$, with $\lambda = 4$, $\mu = 0.5$.

Figure 2 shows the initial temperature distribution (left), and the temperature distribution at $t = 2$ (right), corresponding to the case $z_\infty = -24$, $z_\infty = 7$, $R = 8$, Le $= 0.7$, $\beta = 10$, $\alpha = 0.8$. Notice that, using Fedoseyev's method, the Runge phenomenon has been completely eliminated from the initial profile. Also notice that for $t = 2$, the perturbation to the flame front has disappeared and the flame advances as a plane flame front. In fact, the flame is stable to perturbations whose wavelengths are smaller than $\lambda_0 = 6\pi\sqrt{2} = 26.65$. In the present case $\lambda = 4$ is much smaller than the stability limit λ_0.

If the wavelength of the perturbation is larger than λ_0 the flame front becomes unstable. Figure 3 shows the contour line of temperature $T = 0.5$ at times
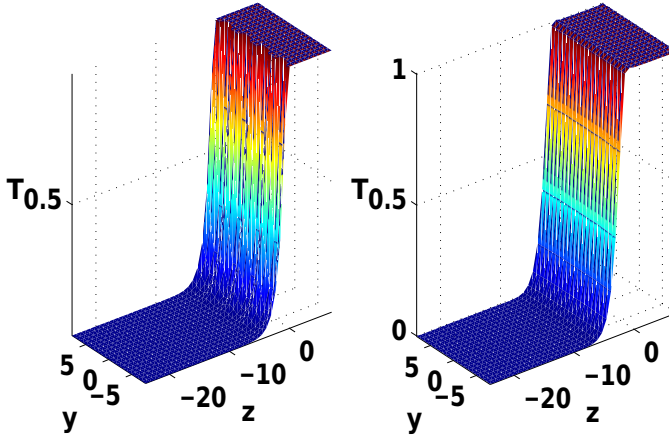
Figure 2: Temperature distribution at $t = 0$ (left) and $t = 2$ (right). $z_{-\infty} = -24$, $z_{\infty} = 7$, $R = 8$, Le $= 0.7$, $\beta = 10$, $\alpha = 0.8$, $n_z = 41$, $n_y = 21$.
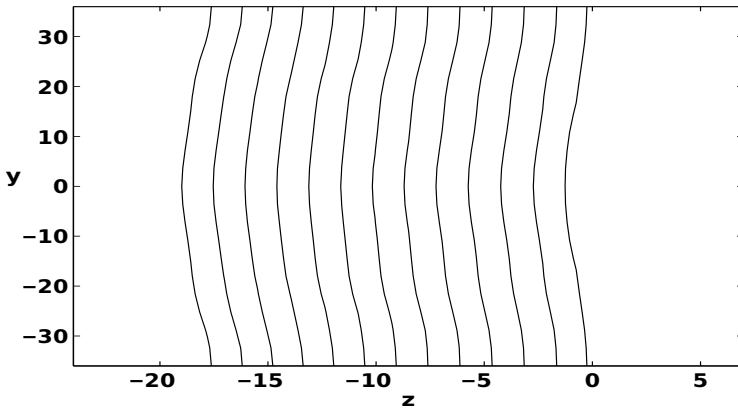

Figure 3: Contour line of temperature $T = 0.5$ for times $t = 0, 1, \ldots, 12$. $z_{-\infty} = -24$, $z_{\infty} = 7$, $R = 36$, Le $= 0.7$, $\beta = 10$, $\alpha = 0.8$, $n_z = 41$, $n_y = 21$.

$t = 0, 1, \ldots, 12$ when the initial flame location $f(y) = \mu \cos(2\pi y / \lambda)$, $\lambda = 72$, $\mu = 0.5$. Notice that in this case the initial perturbation to the flame front does not stabilize but, on the contrary, the amplitude of the perturbation grows with time.

2.1.2 Anchored flame

An interesting problem is to consider a thermally anchored flame. This is achieved by assuming that the channel walls are adiabatic except for $z > z_a$, where the wall is heated to the adiabatic flame temperature ($T = 1$). Moreover, the initially planar flame now tends to draw back towards the hot boundary (on the right) because a flow of fresh mixture is introduced at the left end of the channel. This problem was solved in references [16, 17] using adaptive numerical schemes. For this problem equations (1, 2) are modified by adding to the right-hand side the convective terms $V\, \partial T/\partial z$ and $V\, \partial T/\partial z$ respectively. The velocity V is constant and corresponds to a uniform gas flow in the channel (it has to be large enough to insure that the flame propagates towards the hot boundary). The boundary condition (8) is replaced by

$$
y = \pm R
\begin{cases}
z \leq z_a & \Rightarrow & \dfrac{\partial T}{\partial y}(\pm R, z, t) = 0 \\[2mm]
z > z_a & \Rightarrow & T(x, \pm R, t) = 1 \\[2mm]
& & \dfrac{\partial Y}{\partial y}(\pm R, z, t) = 0
\end{cases}
\tag{17}
$$

We consider the case when the initial flame location is at $z_f = -15$ and a uniform gas flow with speed $V = 2.6$ enters the channel from the left. The lateral wall is kept at $T = 1$ for $z > -10$. A total of $N = 861$ collocation nodes and 897 RBF nodes have been used. The hot wall acts as a flame holder since the fresh mixture cannot cross the hot region without burning. Therefore the boundary of the flame remains attached at $z = -10$ and the flame front eventually converges to a curved steady state.
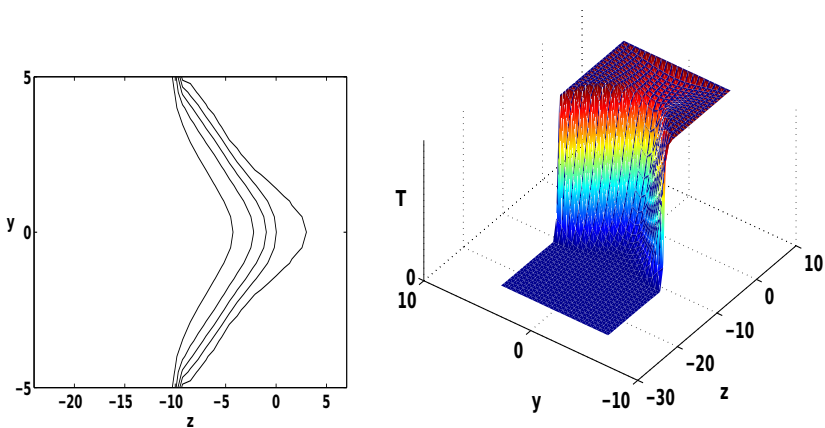

Figure 4: Steady state anchored flame. Left: level curves for $T = 0.1, 0.3, 0.5, 0.7, 0.9$. Right: temperature distribution.

Figure 4 shows the resulting steady state solution for the anchored flame. The left side of the figure shows the level curves and the right side shows the temperature distribution. The curved front can be clearly appreciated.

One of the main advantages of meshless methods is the use of unstructured nodes so that the labor intensive step of mesh generation is avoided. To show the performance of the method when unstructured nodes are used we have solved the anchored flame problem described in the previous Section using the nodes shown in the left side of Figure 5. A total of $N = 501$ collocation nodes and 533 RBF
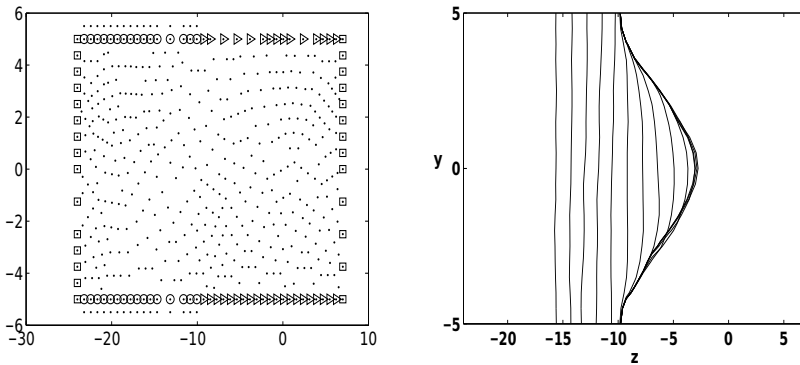

Figure 5: Left: RBF nodes ($\cdot$) and collocation nodes: ($\square$) equation (13), ($\circ$) equation (14), ($\triangleright$) $T = 1$, $\partial Y/\partial y = 0$. Right: Contour line of temperature $T = 0.5$ for times $t = 0, 1, \ldots, 14$. $V = 2.6$, $xa = -10$, $x_{in} = -24$, $x_{out} = 7$, $R = 5$, $Le = 0.7$, $\beta = 10$, $\alpha = 0.8$, $N = 501$.

nodes have been used. The right-hand side of the figure shows the corresponding contour line of temperature $T = 0.5$ at times $t = 0, 1, \ldots, 14$. The flame converges to the same curved steady state which was obtained with structured nodes although a significant smaller number of nodes has been used.

2.2 RBF Finite Difference method (RBF-FD)

In RBF-FD, spatial differential operators appearing in PDEs are approximated by a weighted sum of the values of the sought function at some surrounding nodes. Thus, it can be considered as a generalization of the classical FD method. While in the global method the unknowns are the coordinates of the solution in the functional space spanned by the RBFs, in the local method the unknowns are the values of the solution at the scattered nodes, just the same as with the FD method. However, in the FD method the weights are computed using polynomial interpolation, and in the local RBF one they are computed by fitting an RBF interpolant through its nearest neighbors [7]. In this section we will use Gaussians as RBFs.

2.2.1 Numerical results

We use a coordinate system moving with the flame. To this end, we attach the frame of reference to some point x^* moving with the forefront of the flame with speed $V(t)$. This velocity is determined by imposing at x^* an arbitrary constant temperature. After an initial transient period, the temperature distribution becomes steady in the frame of reference attached to the flame, and the value V (t) becomes stationary. This value is the constant flame speed relative to the wall.

The left side of Figure 6 shows the solution for the case $Le = 1$ and $R = 15$ with isothermal boundary conditions. We use a grid of 91×61 nodes, stencil size $n = 25$, and time step $\Delta t = 10^{-3}$ The flame structure has the so-called mushroom-shape. Notice that the flame extinguishes near the wall and the reaction rate increases smoothly towards the axis of the tube, where the flame structure is almost planar. The right-hand side of the figure shows the corresponding results for $Le = 0.7$ and $R = 20$.
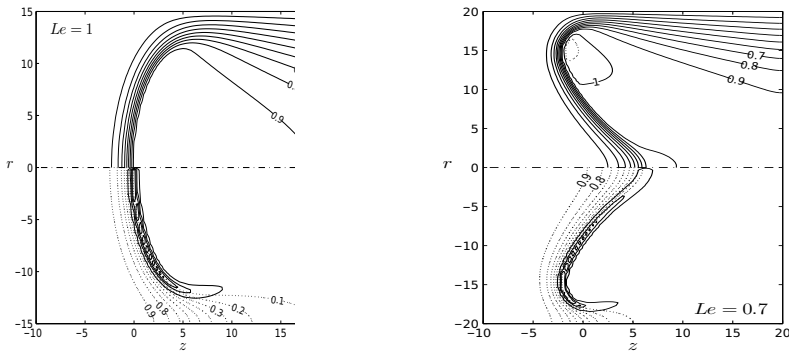

Figure 6: Isothermal wall. Left: $Le = 1$, $R = 15$. Right. $Le = 0.7$, $R = 20$. Upper half: isotherms. Lower half: fuel mass fraction, and reaction rate contours.

Finally, we present the results of solving the three-dimensional model in a duct of radius $R = 8$ with $Le = 0.5$. We have used 6300 nodes, stencil size $n = 35$, and time step size $\Delta t = 0.5 \cdot 10^{-3}$. Figure 7 shows the steady state flame structures computed using isothermal boundary conditions. The left side of the Figure shows the isosurface $T = 0.7$ and the right side shows the longitudinal section of the flame. Both reveal an axisymmetric structure similar to that obtained in the corresponding two-dimensional case.

3 Conclusions

We have analyzed the applicability of the RBF global method to laminar flame propagation modeling. The method is specially well suited to problems with
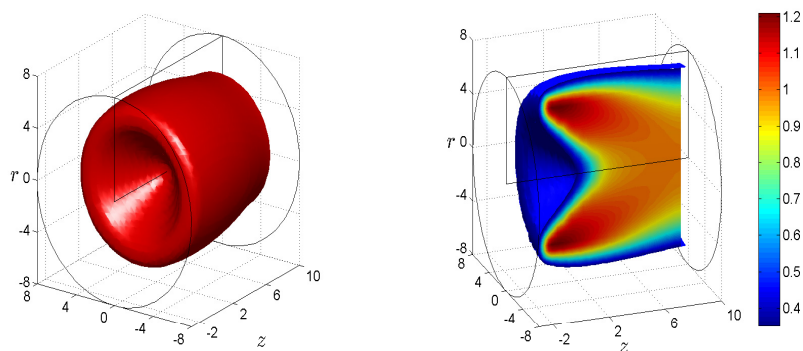
Figure 7: Three-dimensional flame structure for $Le = 0.5$, $R = 8$ and isothermal wall. Left: isosurfaces $T = 0.7$. Right: longitudinal section of the flame.

complex geometries and irregular boundaries where spectral methods can not be applied. An additional advantage is that it is very easy to program and it is independent of the dimension of the problem. Therefore, it is very well suited for solving 3D problems with complex geometries.

References

[1] E. J. Kansa, Multiquadrics, a scattered data approximation scheme with applications to computational fluid dynamics. I. Surface approximations and partial derivatives estimates, Comput. Math. Appl. 19 (1990) 127–145.

[2] E. J. Kansa, Multiquadrics, a scattered data approximation scheme with applications to computational fluid dynamics. II. Solutions to parabolic, hyperbolic and elliptic partial differential equations, Comput. Math. Appl. 19 (1990) 147–161.

[3] C. Shu, H. Ding, and K.S. Yeo, Local radial basis function-based differential quadrature method and its application to solve two-dimensional incompressible Navier-Stokes equations. Comp. Meth. Appl. Mech. & Eng. 192 (2003) 941–954.

[4] A. I. Tolstykh and D. A. Shirobokov, On using radial basis functions in a "finite difference mode" with applications to elasticity problems, Computational Mechanics 33 (2003) 68–79.

[5] G. B. Wright, B. Fornberg, Scattered node compact finite difference-type formulas generated from radial basis functions, J. Comput. Phys. 212 (2006) 99–123.

[6] J.T. Katsikadelis, The 2D Elastostatic Problem in Inhomogeneous Anisotropic Bodies by the Meshless Analog Equation Method (MAEM), Engineering Analysis with Boundary Elements, 32 (2008) 997–1005.

[7] V. Bayona, M. Moscoso, M. Kindelan, Optimal constant shape parameter for multiquadric based RBF-FD method, J. Comput. Phys. 230 (2011) 7384–7399.

[8] W. B. Bush and F. E. Fendell, Asymptotic analysis of laminar flame propagation for general Lewis numbers, Combustion Science and Technology 1 (1970) 421–428.

[9] B. Larrouturou, Adaptive numerical simulation of premixed flame propagation, in Numerical Modeling in Combustion, Ed. T.J. Chung, Taylor & Francis (1993) 133–278.

[10] G. I. Sivashinsky, Non linear analysis of hydrodynamic instability in laminar flame. I - Derivation of basic equations, Acta Astronautica 4 (1977) 1177–1206.

[11] G. I. Sivashinsky, Instabilities, pattern formation and turbulence in flames, Annual Rev. Fluid Mech. 15 (1983) 179–199.

[12] R. L. Hardy, Multiquadric equations of topography and other irregular surfaces, J. Geophys. Res. 176 (1971) 1905–1915.

[13] B. Fornberg and J. Zuev, The Runge phenomenon and spatially variable shape parameters in RBF interpolation, Comput. Math. Appl. 54 (2007) 379–398.

[14] F. Bernal, M. Kindelan, RBF Meshless Modelling of non-Newtonian Hele-Shaw flow, Eng. Anal. Boundary Elements 31 (2007) 863–874.

[15] A. I. Fedoseyev, M. J. Friedman, and E. J. Kansa, *Improved multiquadric method for elliptic partial differential equations via PDE collocation on the Boundary*, Comput. Math. Appl., 43 (2002) 439–455.

[16] F. Benkhaldoun and B. Larrouturou, Explicit adaptive calculations of wrinkled flame propagation, Int. J. Numer. Meth. in Fluids 7 (1987) 1147–1158.

[17] A. Dervieux, B. Larrouturou and R. Peyret, On some adaptive numerical approaches of thin flame propagation problems, Computers & Fluids 17 (1989) 39–60.